Liquid-to-glass transition of tetrahydrofuran and 2-methyltetrahydrofuran*

Tan Rong-Ri(谈荣日)[a)b)c)], Shen Xin(沈 鑫)[a)c)],
Hu Lin(胡 林)[b)], and Zhang Feng-Shou(张丰收)[a)c)d)†]

[a)] *The Key Laboratory of Beam Technology and Material Modification of the Ministry of Education, College of Nuclear Science and Technology, Beijing Normal University, Beijing* 100875, *China*
[b)] *Guizhou Key Laboratory for Photoelectric and Application, College of Science, Guizhou University, Guiyang* 550025, *China*
[c)] *Beijing Radiation Center, Beijing* 100875, *China*
[d)] *Center of Theoretical Nuclear Physics, National Laboratory of the Heavy Ion Accelerator of Lanzhou, Lanzhou* 730000, *China*

(Received 8 March 2012; revised manuscript received 26 May 2012)

Both tetrahydrofuran (THF) and 2-methyltetrahydrofuran (MTHF) are studied systematically at desired temperatures using molecular dynamics simulations. The results show that the calculated densities are well consistent with experiment. Their glass transition temperatures are obtained: 115 K ∼ 130 K for THF and 131 K ∼ 142 K for MTHF. The calculated results from the dipolar orientational time correlation functions indicate that the "long time" behavior is often associated with a glass transition. From the radial and spatial distributions, we also find that the methyl has a direct impact on the structural symmetry of molecules, which leads to the differences of physical properties between THF and MTHF.

Keywords: tetrahydrofuran and 2-methyltetrahydrofuran, glass transition, molecular dynamics simulations

PACS: 64.70.P–, 65.20.Jk, 71.15.Pd **DOI:** 10.1088/1674-1056/21/8/086402

1. Introduction

Recently, great attention is paid to tetrahydrofuran (THF) and 2-methyltetrahydrofuran (MTHF) from both experimental and theoretical aspects as importantly weak polar organic solvents due to their application in chemical synthesis and in spectroscopic studies. As a promising candidate for hydrogen storage,[1,2] THF has already been studied experimentally on the formation of clathrate hydrates. A THF stochastic clathrate hydrate model is supported by X-ray Raman spectra (XRS).[3] For MTHF, the famous structure-H (sH) has been verified by nuclear magnetic resonance (NMR) spectra.[4] Such a new hydrate former can be used for a variety of applications due to high solubility with water. The dynamics of concentration fluctuation in the binary glass has been investigated by X-ray photon correlation spectroscopy[5] revealed that two distinct glass transition temperatures are 129.1 K and 245.1 K in the sample of 40% MTHF/oligomeric methyl metacrylate. The glass transition behavior of neat MTHF[6] has been reported firstly to occur at 91 ± 1 K in liquid. This result was also checked using dielectric spectroscopy[7] and solvation spectroscopy measurement.[8] More importantly, MTHF can provide a cost-effective green alternative to THF as a promising solvent for organometallic reactions[9] and regioselective biotransformations.[10] A recent study[11] reported that MTHF is also a promising candidate to substitute dimethyl sulfoxide (DMSO) or methyl tert-butyl ether (MTBE) in lyase-catalyzed reactions. In fact, MTHF can be easily obtained by hydrogenation from furfural, which is a chemical production isolated from cellulose, hemicelluloses, and lignin such as corn crops or sugar cane bagasse and other plant and agricultural waste. Consequently, MTHF is a more environmentally friendly green solvent and its use can meet the 3R (reduce, recycle, reuse) consideration.

Theoretically, THF was investigated extensively using atomic simulations.[12,13] The stochastic clathrate hydrate model has been confirmed by molec-

*Project supported by the National Natural Science Foundation of China (Grant Nos. 11025524 and 11161130520) and the National Basic Research Program of China (Grant No. 2010CB832903).

†Corresponding author. E-mail: fszhang@bnu.edu.cn

© 2012 Chinese Physical Society and IOP Publishing Ltd

ular dynamics simulations (MD) and density functional theory calculations of XRS.[3] Bedard-Hearn *et al.*[12] found that the relaxation dynamics of all of the rotational and translational degree of freedom of neat THF occur on similar time scales and have similar power spectra, making it impossible to discern by the spectra density analysis which specific molecular motions are involved in solvation. The mixed quantum–classical MD[13] revealed that even at room temperature, the solvation of sodium atoms in THF proceeds in discrete steps, with the number of solvent molecules closest to the atom changing one at a time. At room temperature the symmetry of the tri-iodide ion breaking takes place in ethanol, but not in MTHF. It indicated that the symmetry of solvent molecules affects the solvent frequency shifts and relaxation processes.[14] To apply them better in materials, chemical reaction, and energy sources, different models[15–18] have been proposed to make clear the structural properties of neat THF molecules. Jorgensen and his co-workers[15] firstly developed a united-atom (5-site) model and carried out Monte Carlo (MC) calculations, which displayed it is a reasonable approximation to consider THF as planar. Then, three conformations of THF have been reported by Girard *et al.* in different force fields,[17,18] i.e., the so-called planar, envelope, and twist conformations. They found the twist conformation is the stablest one. However, very few theoretical studies have been performed to analyze the structures and properties of neat MTHF.

In the present paper, we employ MD to calculate primarily the thermodynamic and structural properties of MTHF molecules at desired temperatures, including the density, the self-diffusion coefficient, the dipolar orientational correlation functions, and the radial and spatial distribution functions. For comparison, the corresponding physical properties of THF are calculated. The primary aim is to study the glass transition of THF and MTHF by analyzing the structural and physical properties. This paper is organized as follows. The model and computational details are described in the next section. In Section 3, we display the results of simulations and discuss the thermodynamic properties, the orientational dynamics, and the local structures in details. Conclusions are given in the last section.

2. Model and computational details

THF and MTHF are made up of 13 and 16 atoms, respectively, including oxygen, carbon, and hydrogen atoms. As depicted in Fig. 1, hydrogen is bonded with carbon to form C–H bonds. The carbon atoms on 5-site rings are not in the same plane. The all-atom model is adopted to improve the accuracy of the computer simulations. *Ab initio* quantum chemical calculations are preformed using the restricted Hartree–Fock method (RHF) as described in the program "Guassian 09"[19] to minimize energy and then optimize geometries. The geometries are optimized with 6-31G(d,p) double-zeta basis set in vacuum. During the optimizations, no atoms are hindered to move. The level of convergence for the energy optimization is about 10^{-10} hartree (1 hartree = 27.21 eV). The bond parameters and the atomic charges of stationary conformation from *ab initio* calculations are listed in Table 1.

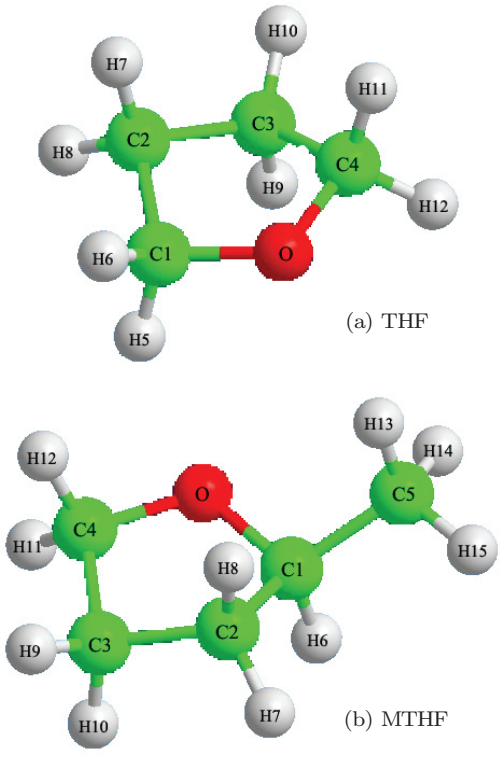


Fig. 1. (colour online) The sketch of the optimized geometries of THF (a) and MTHF (b). The red, green, and grey ball represent oxygen, carbon, and hydrogen atoms, respectively.

Table 1. The bond and Lennard–Jones potential parameters for THF and MTHF, 1 Å = 0.1 nm.

THF and MTHF				THF		MTHF	
	m/g·mol^{-1}	σ/Å	ϵ/K · J · mol^{-1}	Atom species	Q/e	Atom species	Q/e
O	15.9994	3.0041	0.7118	O	−0.34548	O	−0.34537
C	12.0110	3.4001	0.4581	C1	−0.00769	C1	0.08051
H	1.0080	2.5999	0.0628	C2	−0.19765	C2	−0.19307
				C3	−0.19765	C3	−0.19845
Bond lengths/Å		Bond angles/(°)		C4	−0.00769	C4	−0.00759
O–C	1.410	C–O–C	111.5	H5	0.08141	C5	−0.29391
C–C	1.528	O–C–C	104.7 ∼ 109.2	H6	0.10504	H6	0.07400
C–H	1.085	O–C–H	109.0	H7	0.09547	H7	0.10182
		C–C–C	101.6 ∼ 115.7	H8	0.09547	H8	0.09433
		C–C–H	110.0 ∼ 113.8	H9	0.10504	H9	0.10467
		H–C–H	108.0	H10	0.08141	H10	0.09579
				H11	0.09616	H11	0.09359
				H12	0.09616	H12	0.08422
						H13	0.10976
						H14	0.09991
						H15	0.09979

Note: for MTHF, the bond lengths of C1–C5 and C3–C4 are 1.516 Å and 1.532 Å, respectively; the bond angle of C2–C1–C5 is 115.7°. m is the atomic molar mass in units of g·mol^{-1}. Q is the atomic partial charge in e units, i.e., q_m or q_n in Eq. (1), where e is the charge of the proton.

In this study, an empirical potential model is employed to deal with the interactions of molecules. The intermolecular energy expression

$$\phi_{mn} = 4\epsilon_{mn}\left[\left(\frac{\sigma_{mn}}{r_{mn}}\right)^{12} - \left(\frac{\sigma_{mn}}{r_{mn}}\right)^{6}\right] + \frac{q_m q_n}{4\pi\varepsilon_0 r_{mn}} \quad (1)$$

primarily consists of the Lennard–Jones potential energy and the electrostatic interactions. Here, ϵ_{mn} and σ_{mn} are related to the energy and distance scales of the Lennard–Jones (LJ) interactions, which provide short-range intermolecular repulsion and describe the molecular size.[14,20] q_m and q_n are the atomic partial charges which determine the molecular polarity. ε_0 represents the vacuum permittivity and r_{mn} denotes the distance between two atom sites. The LJ potential parameters of the same species atoms derived from *Amber 94*, see Table 1. Interactions between unlike atoms in different molecules can be approximated using the venerable Lorentz–Berthelot mixing rules.[21] The cross terms ϵ_{mn}, σ_{mn} are given by

$$\epsilon_{mn} = \sqrt{\epsilon_{mm} \cdot \epsilon_{nn}}, \quad (2)$$

$$\sigma_{mn} = \frac{\sigma_{mm} + \sigma_{nn}}{2}, \quad (3)$$

where ϵ_{mm} (ϵ_{nn}), σ_{mm} (σ_{nn}) are the LJ potential parameters of the same species atoms, i.e., ϵ and σ in Table 1.

Based on the static conformations obtained from *ab initio* calculations, MD are implemented using the DL_POLY package.[22] In simulations, each cell contains 256 molecules for each simulation and the cubic periodic condition is used to eliminate the boundary effect of surface. The cut-off for the long-range interactions is 12 Å. The Ewald sum method is adopted to treat electrostatic interactions. The intramolecular constrains of the molecules are conserved by using the SHAKE procedure.[23] The time step is 1 fs. Velocities and coordinates of all sites are collected in 100-fs intervals. At the starting point, THF and MTHF molecules are located randomly on two different FCC lattices, and they are heated step by step up to 336 K and 350 K, respectively. At higher temperatures, the static cubic simulation boxes are caused after experiencing 2-ns evolution with the constant-pressure and constant temperature ensemble (NPT) at 1 atm (1 atm = 1.01325×10^5 Pa). Then, the ensembles are changed from NPT to the canonical ensemble (NVT) for improving the efficiency of computer. And the simulations are carried out 2.5 ns after undergoing a pre-equilibration of 100 ps in the NVT ensemble. After the systems are equilibrated, the trajectories of the last 600 ps are collected for data analysis. Then, THF and MTHF systems are in turn annealed to 50 K and 75 K, respectively, within 15 K–25 K intervals. The above simulation processes are reduplicated at desired

temperatures.

3. Results and discussion

3.1. Thermodynamic properties

The glass transition temperature (T_g) is a very useful parameter in estimating the mechanical properties of a material.[24] T_g can be defined by the change in the thermal expansion coefficient which often described by the density (ρ) or the specific volume (V_g). To get a picture of the glass transition behavior, the density ρ and the specific volume V_g are calculated. Figure 2 shows the temperature dependences of the density and the specific volume for THF and MTHF.

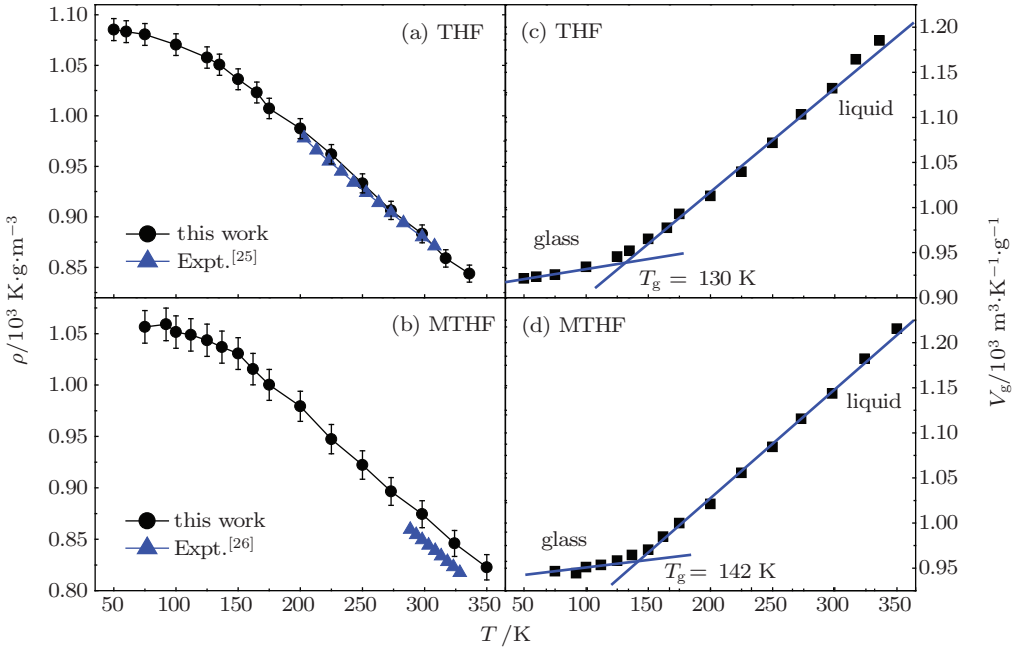


Fig. 2. (colour online) The temperature dependences of the density and the specific volume. In panels (a) and (b), the circle and triangle symbols represent the calculated and experimental densities, respectively. In panels (c) and (d) the blue solid lines are the linear fitting of $V_g \propto T$ in liquid state and glassy state.

It is obvious from Figs. 2(a) and 2(b) that the densities increase with decreasing temperatures for both THF and MTHF. There exist corner points at around 140 K, which divide the curves into two parts with different slopes. The slopes become smaller at the temperatures below 140 K. This indicates that the densities have been little influenced by temperature at the lower temperatures below 140 K. The molecular structures become denser and denser with the temperature decreasing. This reflects the increasing hopping rates of molecular motion above 140 K whereas a slowing down of molecular motion below 140 K. We think that the breakpoints at around 140 K are associated with the glass transition temperatures, which will be described further in the following discussons (Figs. 3–5). At room temperature, the densities of THF and MTHF are $\rho_{\rm THF} = 0.8820$ g/cm^3 and $\rho_{\rm MTHF} = 0.8716$ g/cm^3 which are in good agreement with experiment.[25,26] The relative errors are 0.5% and 2.6%, respectively. The slightly discrepancies between the calculated and experimental values can be explained as follows. The primary reason is that the interaction potentials are just not sufficiently precise to reproduce the correct density. Another one is that the bond parameters are taken from *ab initio* calculations of single-particle gas phases, whereas the present simulations are based on multi-particle liquid phases. By contrast, the atom distances of gas phases are larger than those of liquid phases. Thirdly, THF and MTHF molecules are viewed as rigid body in simulations, which are equivalent to increasing the system volume. Thus, the calculated densities are somewhat smaller than the experimental data.

On the contrary, the V_g decreases nonlinearly as the temperature decreasing, see Figs. 2(c) and 2(d). This change does not occur suddenly, but rather over a range of temperatures which has been called "transformation range". Here T_g is defined by extrapolating

V_g in the glassy state back to the liquid line.[27,28] The $V_g \propto T$ curves in the glassy state and liquid state can be fitted linearly as $V_g = a + bT$, where a, b are the fitting parameters. The horizontal coordinates of the intersection point of the fitting lines are approximatively considered as T_g. As a result, the T_g for THF and MTHF are almost 130 K and 142 K, respectively. Experimentally, although T_g often depends on the cooling rate, the dependence of T_g upon cooling rate is relatively weak. In the present study, we estimate the glass transition temperatures without considering the change of cooling rate in simulations.

The mean square displacement (MSD), is a good measure of the average distance that a given particle in a system travels. Although the MSD gives us information about the atomic diffusion processes in the medium, it is more useful to characterize the glass transition behavior of the system by self-diffusion coefficient D. For a three-dimensional system, D can be written as[21]

$$D = \lim_{t\to\infty} \frac{1}{6Nt} \sum_{i=1}^{N} \langle |\boldsymbol{r}_i(t) - \boldsymbol{r}_i(0)|^2 \rangle = \frac{1}{6} \frac{\mathrm{d}}{\mathrm{d}t} \langle r^2(t) \rangle, \tag{4}$$

where N is the number of particles and $\boldsymbol{r}_i(t) - \boldsymbol{r}_i(0)$ denotes the vector distance traveled by a given particle over the time intervals.

The Arrhenius plots of the self-diffusion coefficient as a function of temperature are shown in Fig. 3. It can be seen clearly that the $\log(D) \propto 1/T$ curves exhibit a break or a step change in the vicinity of the glass transition temperatures. We find the Arrhenius plots go at different linear relations in liquid and glassy state. The different behaviors in the $\log(D) \propto 1/T$ plots reflect different motion modes of molecules in the different states. By extrapolating method,[29,30] we can obtain the glass transition temperatures of THF and MTHF are 115 K and 131 K, respectively.

In contrast, the glass transition temperatures are about 10 K $\sim$ 20 K lower than those obtained from the $V_g \propto T$ curves. Because it is often difficult to make a distinction the accuracy between the two methods, we prefer to the results that $T_g = 115 \sim 130$ K for THF, whereas $T_g = 131 \sim 142$ K for MTHF. This glass transition temperature for MTHF is higher than $T_g = 92$ K confirmed by experiment.[6] The LJ potential maybe responsible for the discrepancy. To diminish the differences between the calculated and experimental data, it is very important to select suitable force field and interaction potential in simulations.

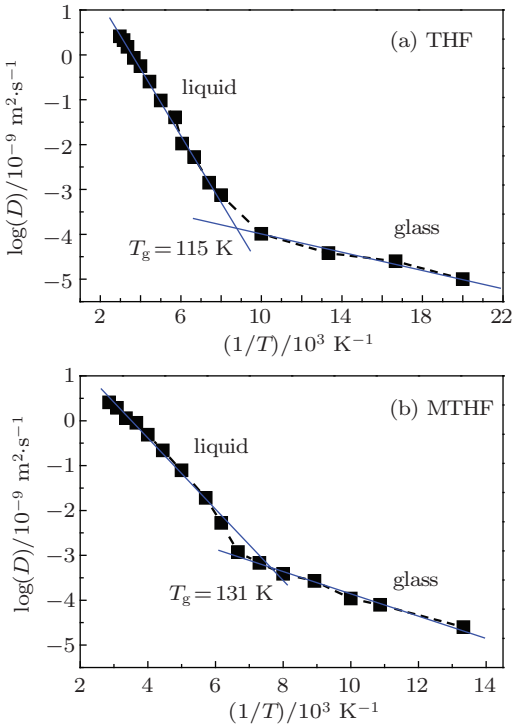


Fig. 3. (colour online) The Arrhenius plots of the self-diffusion coefficient as a function of temperature in THF (a) and MTHF (b). The solid lines are the fitting lines in the liquid and the glassy state.

3.2. Orientational dynamics

The solvation dynamics is often monitored by the decay of solvation time correlation functions.[31] The dipolar orientational time correlation functions ($C_\mu(t)$) describe the orientational motion behaviors and reflect glass transition processes of solvent dynamically. $C_\mu(t)$ can be expressed as[21,32]

$$C_\mu(t) = \frac{\langle \mu_i(t) \cdot \mu_i(0) \rangle}{\langle \mu_i(0) \cdot \mu_i(0) \rangle}, \tag{5}$$

where $\mu_i(t)$ is the dipole moment vector of molecule at time t, and $\langle \mu_i(t) \cdot \mu_i(0) \rangle$ denotes averaging over initial time 0 and over molecules.

The plots of the dipolar orientational correlation functions $C_\mu(t)$ against time for THF and MTHF molecules are shown in Fig. 4. It can be seen obviously that the $C_\mu(t)$s decay with increasing time and the amplitudes of decay are significantly distinct at different temperatures. The higher the temperature climbs, the faster the $C_\mu(t)$ decays. However, the $C_\mu(t) \sim t$ curves are rather gentle at 135 K for THF and at 150 K for MTHF. This indicates the dipolar orientational dynamics are more drastic at higher temperatures and the motions of molecule are restricted at lower temperatures. Compared Fig. 4(a) with Fig. 4(b), it is very clear that the decay of $C_\mu(t)$ for THF are faster

than the ones for MTHF at the same temperatures, and the scales of decay are in tens of picoseconds or hundreds of picoseconds, which signifies the rotational motions of THF molecules are more faster than MTHF. A fairly satisfactory multi-exponential fitting to $C_\mu(t) \sim t$ curves can be described as

$$C_\mu(t) = C_1 \exp(-t/\tau_1) + C_2 \exp(-t/\tau_2), \qquad (6)$$

here τ_1 and τ_2 represent the decay factors of short and long time relaxation behavior, respectively. C_1 and C_2 are the coefficients of the "short time" scale and the "long time" scale. The parameters C_1, C_2, τ_1, and τ_2 are listed in Table 2, where we have also given the average orientational correlation time τ_μ defined by

$$\tau_\mu = \int_0^\infty C_\mu(t)\,\mathrm{d}t. \qquad (7)$$

From Table 2, it can be found that the decay factors of the "long time" scales (τ_2) are longer than the decay factors of the "short time" scales (τ_1) for both THF and MTHF. τ_1 is a few picoseconds and τ_2 is larger than 2 ps. At room temperature, τ_2 is about 11 times larger than τ_1. For THF, τ_2 is 446.0149 ps and around 50 times larger than τ_1 at 135 K, whereas the corresponding datum is 384.7521 ps and about 40 times at 150 K for MTHF. The calculated results are in agreement with Williams' theory,[33] where the "short time" scales of the dipole correlation functions are somewhat arbitrary and the "long time" scales correspond to time greater than about 2 ps. This demonstrates that the "long time" behaviors play a major role in the relaxations, especially at lower temperatures. In fact, the average orientational correlation time τ_μ is a symbol of the relaxation extent. τ_μ is in the scale of picosecond, which suggests that the relaxation is a transient processes.

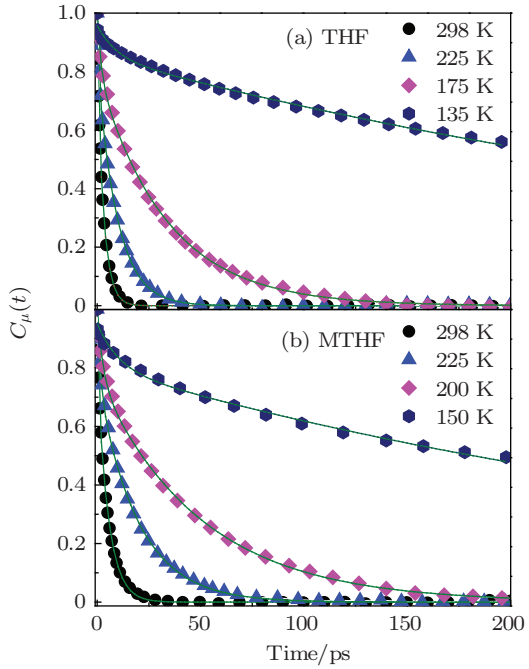


Fig. 4. (colour online) The dipolar orientational correlation functions (solid points with black, blue, magenta, or navy), $C_\mu(t)$, and their fits (solid green lines) for THF (a) and MTHF (b) at different temperatures.

Table 2. The parameters of the fitting to $C_\mu(t) \sim t$ curves presented in Fig. 4.

	Temperature/K	C_1	C_2	τ_1/ps	τ_2/ps	τ_μ/ps
THF	298	0.1761	0.8239	0.3021	3.2131	2.7005
	225	0.1765	0.8235	0.5220	9.6091	8.0081
	175	0.2013	0.7987	1.8376	33.2771	26.9483
	135	0.1478	0.8522	8.9948	446.0149	381.4233
MTHF	298	0.2087	0.7913	0.4551	5.3717	4.3456
	225	0.2382	0.7618	1.4410	19.4858	15.1875
	200	0.2279	0.7721	2.6813	49.8020	39.0632
	150	0.1980	0.8020	10.0649	384.7521	310.5640

Generally speaking, for rotational processes occurring in the "short time" scales, the inertial effects of molecules are of great importance and usually there are not transition of states. On the contrary, for processes occurring in the "long time" scales, the inertial effects are less important and the motions may be associated with the classical reorientation of molecules (or parts of molecules) in Brownian motions. This case is often kept in company with a transition from a state to another.[33] From the point of view, we estimate that a glass transition takes place near 135 K for THF and 150 K for MTHF. Hence, it is easy to understand the fact that the $C_\mu(t)$ decay to zero after experiencing a given time where spanning over 25 ps

to 200 ps (Fig. 4). This is because the dipole moments of THF and MTHF are able to take up all possible orientations in space. Nevertheless, when the temperature declines to near the glass transition temperatures whether for THF or MTHF, the $C_\mu(t)$ actually decay but at a very slow rate. The reason is that the fluidity and the rotational behavior of molecules in the glassy state are much slower than in liquid, in other word, some molecules are confined in glassy state and the vector sums of the dipolar moment vectors are not zero at a short time scale. In practice, the glass transition processes are associated with the reorientation and rearrangement of molecules, and the long-time tail of $C_\mu(t)$ is a direct indicator of the extent of restrictions, with larger value signifying a more restricted environment for molecular reorientation.

3.3. Local structures

The radial distribution functions (RDFs, marked as $g(r)$) are often applied to analyse the structure and the phase transition processes.[34,35] To get a clear picture of the local structure of THF and MTHF, the RDFS of oxygen–oxygen and oxygen–carbon are calculated, and the results are plotted in Figs. 5–7, respectively.

Figure 5 shows the temperature dependences of RDFs (i.e., $g_{\rm OO}(r)$) between two oxygen atoms. At room temperature, a peak is obtained at about 5.65 Å for MTHF, and 4.75 Å for THF, respectively. The latter is different slightly from the result of the classical MC,[15] which hits the peak at around 5.0 Å, see Fig. 5(a). Apart from the inherent limitations of the classical potentials, the possible reason for this disagreement may be the fact that the intramolecular potentials of this work are derived from *Amber 94*, whereas the potential parameters of the classical MC from molecular mechanics (MM2) calculations. Moreover, the charge on the oxygen in this study is 0.35 e, which is different from 0.50 e in the classical MC. At the temperatures higher than 298 K, the peaks of both THF and MTHF have no obvious shift except a little decreasing in intensity, see Figs. 5(b) and 5(c). However, when temperature is below room temperature, the $g_{\rm OO}(r)$ of THF and MTHF shows a different dependence with temperature decreasing from 336 K (for THF) or 350 K (for MTHF) to 75 K. For THF, the peak at 4.75 Å does not shift, but its intensity experiences a distinct increase, as shown in Fig. 5(b). By contrast, the peak of MTHF at 5.65 Å shows a slight increase in intensity, and another peak appears near $r = 4.65$ Å at the temperatures below 150 K, see Fig. 5(c). It demonstrates that the temperature has a great impact on the structures of oxygen–oxygen for MTHF.

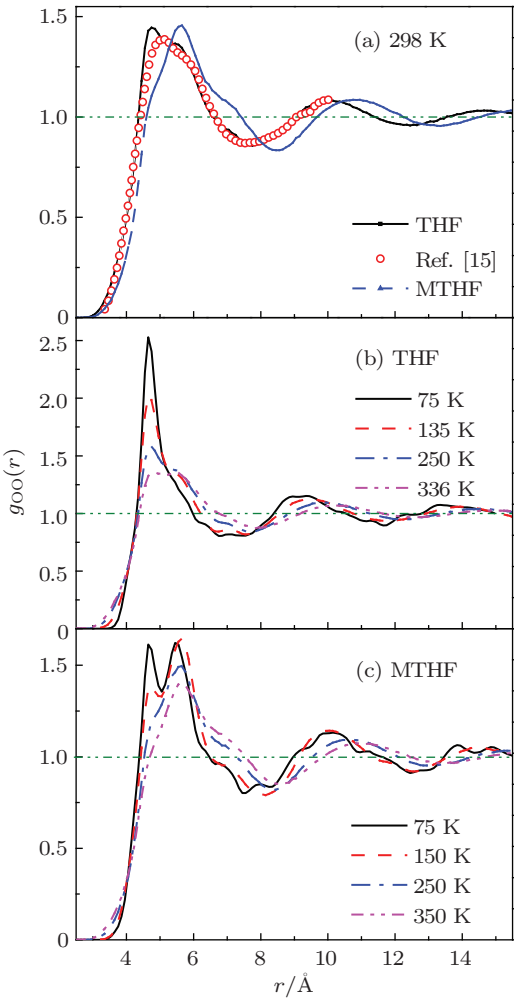


Fig. 5. (colour online) The temperature dependences of the RDFs between two oxygen atoms at room temperature (a). Panels (b) and (c) represent the $g_{\rm OO}(r)$ for THF and MTHF at different temperatures, respectively.

Figures 6 and 7 represent the RDFs between oxygen and carbon groups in THF and MTHF, respectively, including $g_{\rm OC1}(r)$, $g_{\rm OC4}(r)$, and $g_{\rm OC5}(r)$. It is obvious for both THF and MTHF that the structure sharpen with decreasing temperature accompanied by an inward shift slightly of the peak in the RDFs. Compared $g_{\rm OC1}(r)$ with $g_{\rm OC4}(r)$, THF exhibits a quite similar double-peak phenomenon in the regime of $r \leq 8$ Å (Figs. 6(a) and 6(b)), whereas MTHF exhibits a different change, as shown in Figs. 7(a) and 7(b). For THF, the RDFs reaches the first and the second peaks at around 3.65 Å and 5.15 Å, respectively, and the double-peak becomes more pronounced at the tem-

peratures lower than 150 K. The double-peak structures in the RDFs have been explained as no clear structures due to the rather small σ_0 in the previous literatures.[17,18] In our opinions, it seems more reasonable that the orientations of pairs of the closest neighbors molecules are parallel or perpendicular, and the double-peak structures appear when the two orientations are coexist at lower temperatures.

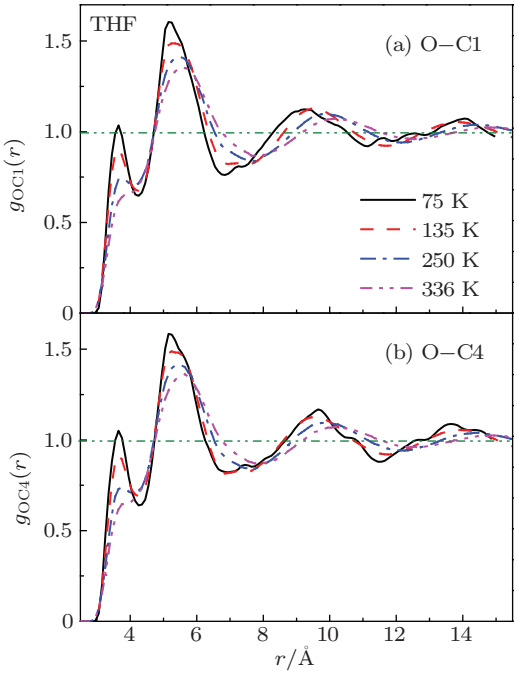


Fig. 6. (colour online) The RDFs $g_{OC1}(r)$ (a) and $g_{OC4}(r)$ (b) between oxygen and carbon groups as a function of temperature for THF.

For MTHF, the $g_{OC1}(r)$ shows a single peak at small r ($r \leq 8$ Å, see Fig. 7(a)), whereas the $g_{OC4}(r)$ shows a distinct double-peak structure (Fig. 7(b)), similar to $g_{OC4}(r)$ of THF in Fig. 6(b). Furthermore, the $g(r)_{OC4}$ are broad with a peak near 3.65 Å, which are not found in the $g(r)_{OC1}$. A close look at Fig. 7(c) reveals that the peak around 3.65 Å of the $g(r)_{OC5}$ diminishes and vanishes finally as increasing temperature, which is quite similar to the $g_{OC4}(r)$ with a maximum near 5.75 Å and the second maximum near 3.65 Å.

Similar temperature dependences of $g_{OC1}(r)$ and $g_{OC4}(r)$ for THF, in part, can be explained by the symmetry of local structure. This symmetrical structure is also checked by the spatial distribution functions (SDFs). As shown in Fig. 8, the center of local coordinate system is set at O site, the X axis goes as a mediana of C1–O–C4 angle, and the Z axis is perpendicular the plane defined by the three sites. Figure 8(a) displays the SDF of O–C1 is same to O–C4 for THF. This indicates the distributions of C1 and C4 atoms are pretty spherically symmetrical. Meanwhile, the approximate planes defined by five-site ring for THF molecules are most likely parallel each other, as presented in the previous references.[16,18] However, for MTHF, the overlap region with the SDF of O–C4 is the one of O–C5, not that of O–C1, as shown in Fig. 8(b). It suggests that the methyl breaks the original symmetry of C1 and C4, and a new structure with the symmetry of C4 and C5 is generated. Besides, the C1 is distributed outward, which signifies the distance of O–C1 is longer than O–C4. It is worth while noting that the temperature has little effect on the distribution of C1 for MTHF. A conclusion may be drawn that the rotations of MTHF molecules are at the center of C1 group, whereas THF molecules rotate round C1 or C4 group.

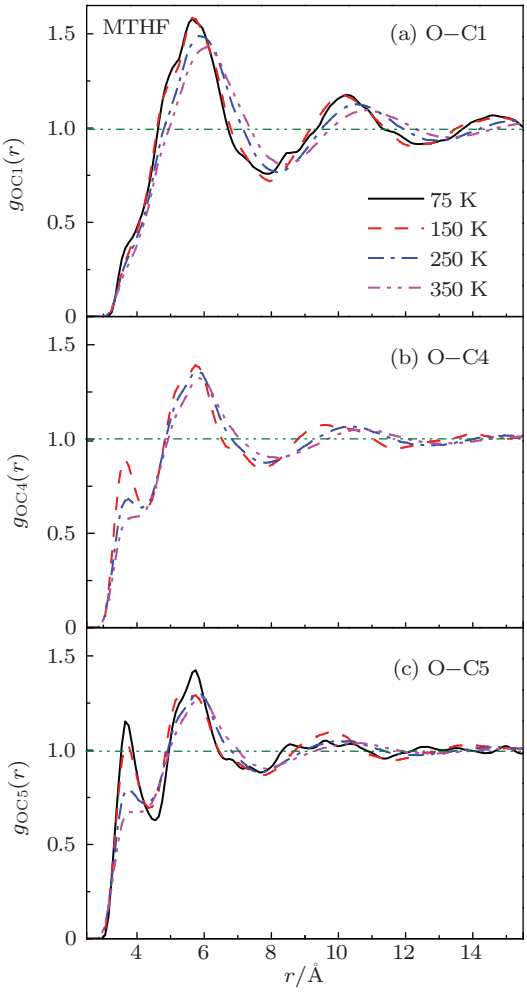


Fig. 7. (colour online) The RDFs $g_{OC1}(r)$ (a), $g_{OC4}(r)$ (b), and $g_{OC5}(r)$ (c) between oxygen and carbon groups as a function of temperature for MTHF.

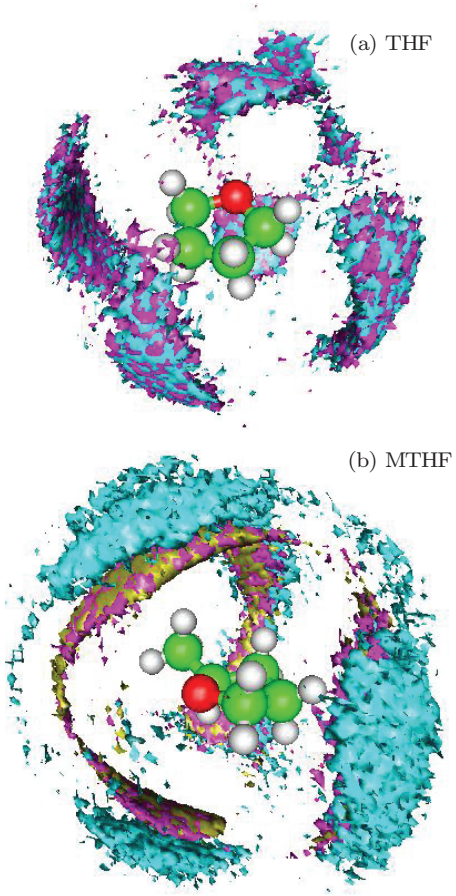


Fig. 8. (colour online) The spatial distribution sketches of O–C1, O–C4, and O–C5 for THF (a) and MTHF (b) at room temperature. The red, green, and grey balls represent oxygen, carbon, and hydrogen atoms, respectively. The cyan, magenta, and dark yellow region denote the possibility of spatial distribution of C1, C4, and C5 around O site.

4. Conclusion

We have investigated the thermodynamic properties of tetrahydrofuran and 2-methyl tetrahydrofuran by molecular dynamics simulations. These structures derived from *ab initio* calculations of gas phase of THF and MTHF have been verified to be basically successful for predicting the thermodynamic properties of their liquid phase. Despite the structures of THF and MTHF are similar to each other except for a methyl bonding to the 5-site ring of MTHF, the thermodynamic properties of MTHF is completely different from those of THF. The calculated results indicate that the densities are in good agreement with experimental data. From the specific volume and the self-diffusion coefficient, we have obtained that the liquid–glass transition occurs between 115 K and 130 K for THF, while the glass transition temperature of MTHF ranges from 131 K to 142 K. At the same time, the present simulations show a strong temperature dependences of the orientational relaxation for THF and MTHF molecules, with shorter dipolar relaxation time implying a quicker rotational behavior happening at higher temperatures. In the dipole time correction function, the "short time" behaviors and the "long time" behaviors are the indicator of different motion mechanism of molecules, and they should be analyzed comprehensively, although the "long time" scales play a critical role in the relaxation of molecules. By analyzing the radial and spatial distributions, one can draw a conclusion that the methyl directly influences the structural symmetry of MTHF molecule which causes the differences between THF and MTHF in the reorientation and rearrangement of molecules when the temperature changes.

It is worthwhile noting that, as a tetrahydrofuran alternative, 2-methyltetrahydrofuran is being promoted as more ecologically friendly green solvent. The present study could provide a good understanding for theoretical studies and practical applications of this organic dipolar aprotic solvents.

Acknowledgements

The authors would like to thank I. T. Todorov, W. Smith and C. W. Yong at the STFC Daresbury Laboratory, UK, for providing the DL_POLY program package and the illuminating discussion.

References

[1] Florusse L J, Peters C J, Schoonman J, Hester K C, Koh C A, Dec S F, Marsh K N and Sloan E D 2004 *Science* **306** 469
[2] Lee H, Lee J W, Kin D Y, Park J, Seo Y T, Zeng H, Moudrakovske I L, Ratcliffe C I and Ripmeester J A 2005 *Nature* **434** 743
[3] Conrad H, Lehmkühler F, Sternemann C, Sakko A, Paschek D, Simonelli L, Huotari S, Feroughi O, Tolan M and Hämäläinen K 2009 *Phys. Rev. Lett.* **103** 218301
[4] Lee J W, Lu H L, Moudrakovski I L, Ratcliffe C I and Ripmeester J A 2010 *J. Phys. Chem.* B **114** 13393
[5] Schramm S, Blochosicz T, Gouirand E, Wipf R, Stühn B and Chushkin Y 2010 *J. Chem. Phys.* **132** 224505
[6] Mizukami M, Fujimori H and Oguni M 1997 *Prog. Theor. Phys. Suppl.* **126** 79
[7] Qi F, EI Goresy T, Böhmer R, Döß A, Diezemann G, Hinze G, Sillescu H, Blochowicz T, Gainaru C, Rössler E and Zimmermann H 2003 *J. Chem. Phys.* **118** 7431
[8] Wendt H and Richert R 2000 *Phys. Rev.* E **61** 1722
[9] Aycock D F 2007 *Org. Process Res. Dev.* **11** 156
[10] Simeó Y, Sinisterra J V and Alcántara A R 2009 *Green Chem.* **11** 855

[11] Shanmuganathan S, Natalia D, van den Wittenboer A, Kohlmann C, Grerner L and de María P D 2010 *Green Chem.* **12** 2240
[12] Bedard-Hearn M J, Larsen R E and Schwartz B J 2003 *J. Phys. Chem.* B **107** 14464
[13] Bragg A E, Glover W J and Schwartz B J 2010 *Phys. Rev. Lett.* **104** 233005
[14] Zhang F S and Lynden-Bell R M 2003 *J. Chem. Phys.* **119** 6119
[15] Chandrasekhar J and Jorgensen W L 1982 *J. Chem. Phys.* **77** 5073
[16] Briggs J M, Matsui T and Jorgensen W L 1990 *J. Comput. Chem.* **11** 958
[17] Faller R, Schmitz H, Blermann O and Müller-Plathe F 1999 *J. Comput. Chem.* **20** 1009
[18] Girard S and Müller-Plathe F 2003 *Mol. Phys.* **101** 779
[19] Frisch M J, Trucks G W, Schlegel H B, *et al.* 2009 *Gaussian 09* Revision A.1 (Wallingford CT: Gaussian, Inc.)
[20] Berendsen H J C, Grigera R J and Straatsma T P 1987 *J. Phys. Chem.* **91** 6269
[21] Allen M P and Tildesley D J 1987 *Computer Simulation of Liquids* (Oxford: Clarendon Press)
[22] Todorov I T and Smith W 2010 *DL_POLY-4.02* (STFC Daresbury Laboratory, Warrington WA44AD, Cheshire, UK)
[23] Miyamoto S and Kollman P A 1992 *J. Comput. Chem.* **13** 952
[24] Hou Z Y, Liu R S, Tian Z A and Wang J G 2011 *Chin. Phys.* B **20** 066102
[25] Carvajal C, Tölle K J, Smid J and Szwarc M 1965 *J. Am. Chem. Soc.* **87** 5548
[26] Vallés C, Pérez E, Mainar A M, Santafé J and Domínguez M 2006 *J. Chem. Eng. Data* **51** 1105
[27] Ediger M D, Angell C A and Nagel S R 1996 *J. Phys. Chem.* **100** 13200
[28] Debenedetti P G and Stillinger F H 2001 *Nature* **410** 259
[29] Liu J, Wang S Y, Zhang C P, Xin L J, Wnag D and Sun M H 2007 *Chin. Phys. Lett.* **24** 2025
[30] Habasaki J and Ngai K L 2008 *Anal. Sci.* **24** 1321
[31] Choudhury N and Pettitt B M 2005 *J. Phys. Chem.* B **109** 6422
[32] Pal S, Balasubramanian S and Bagch B 2002 *J. Chem. Phys.* **117** 2852
[33] Williams G 1972 *Chem. Rev.* **72** 55
[34] Liu C S, Liang Y F, Zhu Z G and Li G X 2005 *Chin. Phys.* **14** 785
[35] Li L, Shao J L, Duan S Q and Liang J Q 2011 *Chin. Phys.* B **20** 046402